

Berry phase mediated topological thermoelectric transport in gapped single and bilayer graphene

Chuanwei Zhang¹, Sumanta Tewari², and S. Das Sarma³

¹*Department of Physics and Astronomy, Washington State University, Pullman, WA 99164*

²*Department of Physics and Astronomy, Clemson University, Clemson, SC 29634*

³*Condensed Matter Theory Center, Department of Physics, University of Maryland, College Park, MD 20772*

We consider the anomalous thermoelectric transport in gapped single and bilayer graphene where the gap may be due to broken inversion symmetry. In the presence of the gap, non-trivial Berry phase effects can be shown to mediate a transverse thermoelectric voltage in response to an applied temperature gradient even in the absence of a perpendicular magnetic field. This spontaneous, anomalous Nernst effect is nonzero for non-uniform chemical potential in the two inequivalent valleys in the graphene band structure. Conversely, the Nernst response can be used to create a valley-index polarization between the two transverse sample edges as in the analogous valley Hall effect.

PACS numbers: 73.63.-b, 72.15.Jf

I. INTRODUCTION

Interesting electric transport properties of the Dirac quasiparticles of graphene have recently come under focus.^{1,2,3,4,5} Graphene, which consists of a single layer of carbon atoms in a bi-partite honeycomb lattice, has a unique band structure that includes two inequivalent valleys in the first Brillouin zone of the momentum space. In gapless graphene, the valleys are characterized by the conduction and the valence bands touching each other at zero energy. Near the valleys, the appropriate quasiparticle dispersion relations are linear in momentum, similar to those of massless Dirac quasiparticles. Inter-valley-scattering is generally suppressed^{6,7,8}, and will be ignored here, due to the absence of a large enough scattering wavevector mixing the two Dirac points.

In some graphene samples, e.g., epitaxial graphene on SiC substrate, a sizable gap has been reported⁹ in the quasiparticle spectrum near the Dirac points. Since the gap approaches zero with increasing sample thickness, it has been attributed to the effects due to the substrate, which is believed to break the sublattice (hence, the space inversion (SI)) symmetry.⁹ Note that a quasiparticle gap in graphene can also result from confined geometries such as in the graphene nanoribbons.^{10,11} In bilayer graphene, an applied interlayer voltage bias can lead to a gap due to broken SI symmetry.¹² In such systems, the effects of the momentum space Berry curvature,¹³ which is sharply peaked at the two valleys, give rise to non-trivial, topological, electric transport phenomena.^{14,15} In this paper, we discuss the effects of the topological Berry phases on another class of transport coefficients, the thermoelectric response coefficients. We will focus, in particular, on the topological Nernst effect of gapped graphene. In light of the recent successful measurements of the regular thermoelectric coefficients in graphene,^{16,17,18} the anomalous, topological Nernst response we discuss here acquires particular relevance and importance. Although the specific calculations in this paper apply to graphene samples with broken SI symmetry, they should, more generally, be qualitatively valid in the presence of a gap of any origin near the Dirac points. Note that an energy gap is ultimately essential for use of graphene as an electronic material.

We calculate the Berry phase supported, spontaneous (*i.e.*,

it exists even without an external magnetic field) Nernst effect of the low energy quasiparticles in graphene, and show that it is non-zero for a non-zero valley polarization in the sample. While a non-zero valley polarization can be artificially created,¹⁹ it can also be induced by an applied magnetic field itself in a generic Nernst measurement set up.¹⁵ The regular Nernst effect in gapped graphene may, therefore, have a substantial anomalous contribution because of the induced valley polarization. Even in the absence of any valley polarization, the spontaneous Nernst signals are non-zero from the individual valleys, but are equal and opposite to each other so the total signal is zero. Therefore, they can be used to create a non-zero valley polarization on the transverse edges, which can be technologically important.

In recent experiments, thermoelectric coefficients, in particular, the Nernst coefficient, have been measured for non-zero transverse magnetic fields in gapless graphene.^{16,17,18} The topological Nernst effect we discuss here exists even in the absence of any external magnetic field; it is solely driven by the effective magnetic field, given by the Berry curvature, near the valley centers in the momentum space. In the thermoelectric experiments, a temperature gradient $-\nabla T$, applied along, say, the \hat{x} direction produces a measurable transverse electric field. The total charge current in the presence of the electric field \mathbf{E} and $-\nabla T$ is given by $J_i = \sigma_{ij} E_j + \alpha_{ij} (-\partial_j T)$, where σ_{ij} and α_{ij} are the electric and the thermoelectric conductivity tensors, respectively. Setting \mathbf{J} to zero, the Nernst signal, defined as $e_N \equiv E_y / |\nabla T| = \rho \alpha_{xy} - S_{xx} \tan \theta_H$, is measured, where α_{xy} is the Nernst conductivity defined via the relation $J_x = \alpha_{xy} (-\partial_y T)$ in the absence of the electric field, $\rho = 1/\sigma_{xx}$ is the longitudinal resistance, $S_{xx} = E_x / |\nabla T| = \rho \alpha_{xx}$ is the thermopower, and $\tan \theta_H = \sigma_{xy} / \sigma_{xx}$ is the Hall angle. If the second term is small, which is sometimes the case,²⁰ $\rho \alpha_{xy}$ completely defines the Nernst signal, but in the most general case one should extract α_{xy} from the experimental data to compare with our calculations.

In this paper, the Berry phase mediated topological contribution to α_{xy} is calculated through two different approaches. In the first, path integral, method, we first compute the frequency-dependent off-diagonal component of the electric conductivity tensor, $\sigma_{ij}(\Omega)$, for the Dirac quasiparticles in graphene. At low temperatures, the Nernst conductivity α_{xy}

can be related to the zero temperature DC Hall conductivity σ_{xy} through the Mott relation,²¹ Eq. (22). This method has the advantage that it produces, as a by-product, the imaginary part of the AC Hall conductivity, σ''_{xy} , which can be related to the possible polar Kerr effect^{22,23} in graphene. Indeed, in the case of a non-zero valley-index polarization in the sample, the Berry phase induced polar Kerr effect will be non-zero and observable. Another advantage of this method is that it can give a neat analytical expression of the Nernst conductivity at low temperatures. The effects of quasiparticle nonlinear dispersion relations on the topological transport properties of graphene have also been discussed in this framework. This method, however, is approximate, and gives the values of the Nernst coefficient only at low enough temperatures. In a more general method, which is valid also at higher temperatures, the anomalous contribution to α_{xy} can be calculated from the coefficient $\bar{\alpha}_{xy}$, which determines the transverse heat current \mathbf{J}^h in response to an electric field \mathbf{E} : $J_x^h = \bar{\alpha}_{xy} E_y$. The coefficients are related by one of the Onsager relations: $\bar{\alpha}_{xy} = T\alpha_{xy}$.^{24,25} This way of computing α_{xy} makes use of the Berry curvature in the graphene band structure (see Eq. (24)) more directly. It is a much more general method, which we have used in our plots for the Nernst coefficient as a function of temperature in Figs. 2 and 3. Using this method, we have been able to go beyond the linear temperature dependence arising out of the Mott relation.

The paper is organized as follows: Sec. II gives the Dirac-like Hamiltonian for single layer graphene. Section III is devoted to the topological Hall conductivity of single layer graphene. We calculate the AC Hall conductivity $\sigma_{ij}(\Omega)$ using the path integral approach and discuss the possible polar Kerr effect for single layer graphene. In the limit $\Omega = 0$, we obtain the DC Hall conductivity. The effects of nonlinear quasiparticle dispersion relation on the Hall conductivity are also discussed. In Sec. V, we calculate the topological Nernst conductivity α_{xy} via both the Mott relation and the transverse heat current coefficient. We do this for both single and bilayer graphene. Finally, Section VI is devoted to the conclusion.

II. DIRAC-LIKE HAMILTONIAN

In the tight-binding approximation, graphene single layer with staggered sublattice potential (which breaks the space inversion symmetry) can be modeled with the nearest-neighbor hopping energy t and a site energy difference Δ between the sublattices,²⁶

$$H = \begin{pmatrix} \Delta/2 & \zeta(\mathbf{p}) \\ \zeta^*(\mathbf{p}) & -\Delta/2 \end{pmatrix}, \quad (1)$$

where

$$\begin{aligned} \zeta(\mathbf{p}) &= -t \sum_i e^{i\mathbf{p}\cdot\delta_i} \\ &= -te^{ip_x a/2} \left[2 \cos\left(\frac{\sqrt{3}p_y a}{2}\right) + e^{-i3p_x a/2} \right] \end{aligned} \quad (2)$$

with $\delta_{1,2} = \frac{a}{2}(1, \pm\sqrt{3})$, $\delta_3 = a(-1, 0)\hat{x}$, a is the lattice constant. The Hamiltonian (1) operates on the two-component spinor $\hat{\Psi}_{\mathbf{p}} = (\hat{c}_{A\mathbf{p}}, \hat{c}_{B\mathbf{p}})$, where $\hat{c}_{A\mathbf{p}}, \hat{c}_{B\mathbf{p}}$ denote the annihilation operators on the two sublattices A, B. The most interesting physics occurs around two valleys located at the Brillouin zone corners $\mathbf{K}_{1,2} = \frac{4\pi}{3\sqrt{3}a}(0, \tau_z)$, where $\tau_z = \pm 1$ labels the two valleys. Denoting $\mathbf{k} = \mathbf{p} - \mathbf{K}_{1,2}$ to measure the momentum from the valley centers, we can rewrite the Hamiltonian (1) as

$$H = \frac{\Delta}{2}\sigma_z + \zeta_1(\mathbf{k})\sigma_x + \zeta_2(\mathbf{k})\sigma_y. \quad (3)$$

Here

$$\zeta_1(\mathbf{k}) = -t \left[2 \cos\frac{k_x a}{2} \cos\left(\frac{2\pi}{3}\tau_z + \frac{\sqrt{3}k_y a}{2}\right) + \cos(k_x a) \right], \quad (4)$$

$$\zeta_2(\mathbf{k}) = t \left[2 \sin\frac{k_x a}{2} \cos\left(\frac{2\pi}{3}\tau_z + \frac{\sqrt{3}k_y a}{2}\right) - \sin(k_x a) \right]. \quad (5)$$

The spectrum of the Hamiltonian consists of two branches with the eigenenergies $E_{\pm}(\mathbf{k}) = \pm\Lambda(\mathbf{k})$, where

$$\begin{aligned} \Lambda(\mathbf{k}) &= \left[t^2 \left(1 + 4 \cos^2 \Theta + 4 \cos \Theta \cos \frac{3k_x a}{2} \right) + \frac{\Delta^2}{4} \right]^{\frac{1}{2}} \quad (6) \\ \Theta &= \frac{2\pi}{3} + \frac{k_y a \sqrt{3}}{2} \tau_z. \end{aligned}$$

Close to the valley centers, we can expand $\zeta_1(\mathbf{k})$ and $\zeta_2(\mathbf{k})$ to the first order in \mathbf{k} , and rewrite the Hamiltonian as

$$\hat{H} = \frac{\Delta}{2}\sigma_z + \frac{3at}{2}(\tau_z k_y \sigma_x - k_x \sigma_y) = \mathbf{\Lambda}(\mathbf{k}) \cdot \boldsymbol{\sigma}, \quad (7)$$

with $\Lambda_1 = 3at\tau_z k_y/2$, $\Lambda_2 = -3atk_x/2$, $\Lambda_3 = \Delta/2$. The energy spectrum becomes

$$\Lambda(\mathbf{k}) = |\mathbf{\Lambda}(\mathbf{k})| = \frac{\sqrt{\Delta^2 + 9a^2 t^2 k^2}}{2}. \quad (8)$$

III. HALL CONDUCTIVITY

A. AC Hall conductivity

Introducing the Lagrangian density, $\mathcal{L} = i\omega_n \hat{I} - \hat{H}(\mathbf{k})$, where ω_n is a fermionic Matsubara frequency, we obtain the electron Green's function (for a single valley) as a function of $\vec{k} = (i\omega_n, k_x, k_y)$

$$G_0(\vec{k}) = \mathcal{L}^{-1} = \frac{i\omega_n \hat{I} + \mathbf{\Lambda}(\mathbf{k}) \cdot \hat{\sigma}}{g(\omega_n, \mathbf{k})}. \quad (9)$$

Here $g(\vec{k}) = (i\omega_n)^2 - |\mathbf{\Lambda}(\mathbf{k})|^2$. In order to calculate the AC Hall conductivity, we consider the electromagnetic potential $\vec{A} = (A_0, A_x, A_y)$, where A_0 is the scalar potential, and $\mathbf{A} = (A_x, A_y)$ is the vector potential. Expanding \mathcal{L} to

the first order in \vec{A} , and integrating out the fermions, we identify the coefficient of the Chern-Simons-like term in the effective action as the anomalous AC Hall conductivity for a single valley,²³

$$\sigma_{xy}(\Omega_m) = \sum_{\vec{k}} \frac{\Upsilon(\mathbf{k})}{g(\omega_n, \mathbf{k}) g(\omega_n + \Omega_m, \mathbf{k})}, \quad (10)$$

$$\Upsilon(\mathbf{k}) = -2\mathbf{\Lambda} \cdot \left[\frac{\partial \mathbf{\Lambda}}{\partial k_x} \times \frac{\partial \mathbf{\Lambda}}{\partial k_y} \right]. \quad (11)$$

Here the electromagnetic potential $\vec{A}(\vec{q})$ was assumed to be a function of the Fourier variables $\vec{q} = (i\Omega_m, q_x, q_y)$, with Ω_m a bosonic Matsubara frequency, and we took the limit $\mathbf{q} \rightarrow 0$ to arrive at Eq. (10). Substituting the expression for $\mathbf{\Lambda}(\mathbf{k})$ from the Hamiltonian (7) into the formula (11), we find

$$\Upsilon(\mathbf{k}) = \frac{-9\tau_z a^2 t^2 \Delta}{4}. \quad (12)$$

Summing over the fermionic Matsubara frequency ω_n in Eq. (10) and analytically continuing to the real bosonic frequency, $i\Omega_m \rightarrow \Omega + i\delta$, where δ is a positive infinitesimal, we find,

$$\sigma_{xy}(\Omega) = \int \frac{d^2\mathbf{k}}{(2\pi)^2} \frac{\Upsilon(\mathbf{k}) \{f[E_+(\mathbf{k}) - \mu] - f[E_-(\mathbf{k}) - \mu]\}}{\Lambda(\mathbf{k}) [\Omega + i\delta - 2\Lambda(\mathbf{k})] [\Omega + i\delta + 2\Lambda(\mathbf{k})]}. \quad (13)$$

Here $f(E - \mu)$ is the Fermi occupation function at temperature T and μ is the chemical potential. The minus sign between the two Fermi functions is due to the opposite sign of the Berry curvature for the conduction and the valence bands of electrons. Since $\Lambda(\mathbf{k}) = \sqrt{\Delta^2 + 9a^2 t^2 k^2}/2$ and $\Upsilon(\mathbf{k})$ are constants, we can define $\varepsilon = k^2/2$ and change the integration to

$$\sigma_{xy}(\Omega) = \int_0^\infty \frac{d\varepsilon}{2\pi} \frac{\Upsilon F(\mu)}{E(\varepsilon) [\Omega + i\delta - 2E(\varepsilon)] [\Omega + i\delta + 2E(\varepsilon)]}, \quad (14)$$

where $E(\varepsilon) = \frac{1}{2}\sqrt{\Delta^2 + 18a^2 t^2 \varepsilon}$, $F(\mu) = \{f[E(\varepsilon) - \mu] - f[-E(\varepsilon) - \mu]\}$.

It is clear that if the two valleys have the same chemical potential, $\mu_{K_1} = \mu_{K_2}$, the total AC Hall conductivity $\sigma_{xy}^t(\Omega) = \sigma_{xy}^{K_1}(\Omega) + \sigma_{xy}^{K_2}(\Omega) = 0$, because of the opposite signs of the function Υ for the two valleys. However, the Hall current for an individual valley is nonzero.

The imaginary part of the AC Hall conductivity, $\sigma_{xy}''(\Omega)$, comes from the pole in Eq. (13) at $\Omega = 2E(\varepsilon)$. This pole represents vertical interband transitions induced by the electromagnetic wave. Taking the imaginary part of (13), we find

$$\sigma_{xy}''(\Omega) = -\frac{\Upsilon e^2}{\pi \Omega^2 \hbar} \int_0^\infty d\varepsilon \delta[\Omega - 2E(\varepsilon)] F(\mu). \quad (15)$$

Here we have already taken into account the spin degeneracy. At $T = 0$, $F(\mu) = 0$ if $E(\varepsilon) < \mu$ and $F(\mu) = 1$ for $E(\varepsilon) > \mu$. Therefore, if $\Omega < 2\mu$ or $\Omega < \Delta$, $\sigma_{xy}''(\Omega) = 0$. If $\Omega \geq 2\mu$ and $\Omega \geq \Delta$, we have

$$\sigma_{xy}''(\Omega) = \frac{e^2 \Delta}{2\hbar \Omega}. \quad (16)$$

At finite temperatures, we have $\sigma_{xy}''(\Omega) = \frac{\Delta e^2}{2\hbar \Omega} F(\mu)$ if $\Omega \geq \Delta$. For unequal population of the quasiparticles in the two valleys, the imaginary part of the AC Hall conductivity is non-zero. Since the polar Kerr angle, θ_K , which is the angle of rotation of the plane of polarization of a linearly polarized light on normal reflection from the sample, is directly proportional to $\sigma_{xy}''(\Omega)$ ^{22,23}, in this case, there will be a non-zero polar Kerr effect in graphene.

B. DC Hall conductivity

Taking $\Omega = 0$ in Eq. (13), we have for the DC Hall conductivity,

$$\sigma_{xy}(0) = - \int \frac{d^2\mathbf{k}}{(2\pi)^2} \frac{\Upsilon F(\mu)}{4\Lambda^3(\mathbf{k})}. \quad (17)$$

Notice that

$$\Pi = -\frac{\Upsilon}{4\Lambda^3(\mathbf{k})} = \frac{9a^2 t^2 \Delta \tau_z}{2(\Delta^2 + 9a^2 t^2 k^2)^{3/2}} \quad (18)$$

is just the Berry curvature for an individual valley¹⁵. We see that the Berry curvatures for the two valleys differ only by a sign. At zero temperature and $\mu = 0$, $\sigma_{xy}(0) = -\tau_z/4\pi$. We should multiply the result by two to take account of spin degeneracy. Restoring e and \hbar , we have (for a single valley)

$$\sigma_{xy}(0) = -e^2 \tau_z / h. \quad (19)$$

For nonzero $\mu > \Delta/2$, i.e., μ lying in the conductance band,

$$\sigma_{xy}(0) = -\tau_z e^2 \Delta / 2h\mu. \quad (20)$$

As μ becomes very big, $\sigma_{xy}(0)$ again becomes zero.

C. Nonlinear spectrum

The form of the Berry curvature (18) $\Pi = -\frac{\Upsilon}{4\Lambda^3}$ also applies to the general Hamiltonian (3) without the linear approximation (i.e., the Hamiltonian (7)). In this case, we should use $\mathbf{\Lambda}$ determined by Eq. (6). It is easy to show that

$$\Upsilon(\mathbf{k}) = -\frac{\sqrt{3}a^2 t^2 \Delta \tau_z}{2} \left[\frac{2 \cos(\frac{\pi}{6} + \frac{\sqrt{3}k_y a}{2} \tau_z) \cos(\frac{3k_x a}{2})}{+ \cos(\frac{\pi}{6} - \sqrt{3}k_y a \tau_z)} \right]. \quad (21)$$

The lowest order in \mathbf{k} (i.e., $\mathbf{k} = \mathbf{0}$) of (21) yields Eq. (12). In the presence of the nonlinear part of the spectrum, the symmetry relation between the Berry curvatures in the two valleys is given by $\Pi_{K_1}(\mathbf{k}) = -\Pi_{K_2}(-\mathbf{k})$, and the total Nernst conductivity will be non-zero only for non-zero valley polarization. In Fig. 1a, we plot the Berry curvature around the valley center \mathbf{K}_2 ($\tau_z = -1$). We see that the Berry curvature is very small for a large \mathbf{k} . Therefore, the large \mathbf{k} regimes give very little contribution to the transport quantity of graphene. In fact, for $(k_x a, k_y a) = (\frac{\pi}{36}, \frac{\pi}{36})$, the Berry curvature is only

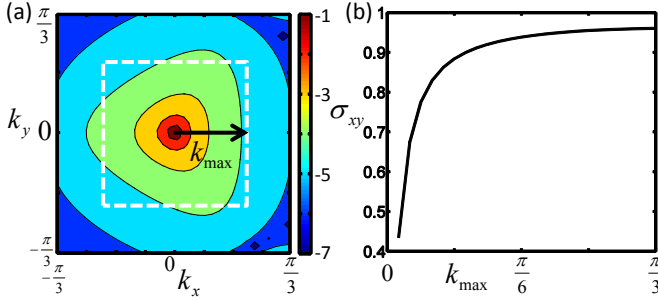


FIG. 1: (Color online) (a) Berry curvature Π (we plot $-\Pi$ for convenience) around the valley center K_2 . $t = 2.8eV$, $\Delta = 0.26eV$. The plot is in the logarithm scale. The dashed line indicates the integration region for (b). (b) Plot of the DC conductivity with different integration region $-k_{\max} \leq k_x, k_y \leq k_{\max}$. The unit of $\sigma_{xy}(0)$ is e^2/h .

1% of its peak value. In Fig. 1b, we plot the DC Hall conductivity at $T = 0$ and $\mu = 0$, taking account of the nonlinear spectrum. Because of the nonlinear spectrum, we cannot take the integration region up to $k = \infty$, the limit that is used for the linear spectrum. However, the DC Hall conductivity $\sigma_{xy}(0)$ at each valley is still very close to $-e^2\tau_z/h$ (the value in Eq. (19) obtained using the linear spectrum) for a reasonably large integration region. Therefore the nonlinear spectrum does not play an important role on the anomalous topological transport properties of graphene, and will be neglected in the following.

IV. ANOMALOUS NERNST EFFECT

A. Single layer graphene

Since the transverse Hall conductivity can be non-zero for gapped graphene, it is natural to ask whether there exists an anomalous Nernst effect. For this purpose, at low temperatures, we can use the Mott relation²¹,

$$\alpha_{xy} = -\frac{\pi^2 k_B^2}{3e} \frac{d\sigma_{xy}}{d\mu} T. \quad (22)$$

For $-\Delta/2 < \mu < \Delta/2$, i.e., μ falling in the band gap, σ_{xy} is independent of μ , and we have $\frac{d\sigma_{xy}}{d\mu} = 0$. Thus, $\alpha_{xy} = 0$. If $\mu \geq \Delta/2$, we have

$$\frac{d\sigma_{xy}}{d\mu} = \frac{\tau_z e^2 \Delta}{2h\mu^2}. \quad (23)$$

Similarly, for $\mu \leq -\Delta/2$, $\frac{d\sigma_{xy}}{d\mu} = -\tau_z \frac{e^2}{h} \frac{\Delta}{2\mu^2}$. We see that α_{xy} is discontinuous at $\mu = \pm\Delta/2$.

More generally, the anomalous contribution to α_{xy} can be calculated from the transverse heat current coefficient $\bar{\alpha}_{xy}$. This way of computing α_{xy} makes direct use of the Berry curvature in the graphene band structure. In the presence of the Berry curvature and the electric field, the electron velocity acquires the additional anomalous term $\hbar\mathbf{v}_{\mathbf{k}} = e\mathbf{E} \times \Pi(\mathbf{k})$ ²⁷.

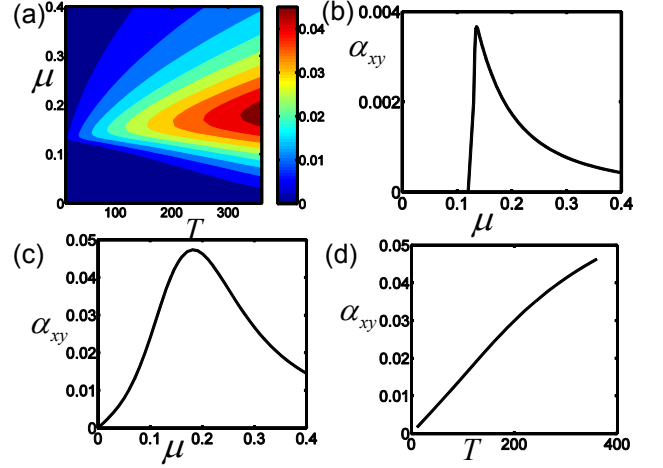


FIG. 2: (Color online) Anomalous Nernst signal for a single valley for single layer graphene. The units for μ , T , and α_{xy} are eV, K, and $k_B e/h$, respectively. The parameters $t = 2.82eV$, $\Delta = 0.26eV$. (a) Contour plot for α_{xy} . (b) Plot of α_{xy} with respect to μ for $T = 11.6$ K. Note the discontinuity at $\mu = \Delta/2$, as predicted by the Mott relation. The decay for $\mu > \Delta/2$ follows $\sim 1/\mu^2$. (c) Plot of α_{xy} with respect to μ for $T = 360$ K. Note the disappearance of the discontinuity. (d) Plot of α_{xy} with respect to T for $\mu = 0.2$ eV.

This velocity multiplied by the entropy density produces the transverse heat current coefficient²⁸:

$$\bar{\alpha}_{xy} = T\alpha_{xy} = \frac{2e}{\beta\hbar} \sum_n \int \frac{d^2\mathbf{k}}{(2\pi)^2} \Pi_n(\mathbf{k}) s_n(\mathbf{k}). \quad (24)$$

Here $s(\mathbf{k}) = -f_{\mathbf{k}} \ln f_{\mathbf{k}} - (1 - f_{\mathbf{k}}) \ln(1 - f_{\mathbf{k}})$ is the entropy density of the electron gas, $f_{\mathbf{k}} = f[E_n(\mathbf{k})]$ is the Fermi distribution function, and the sum is taken over both bands. This formula for α_{xy} , which we use in the figures 2 and 3, coincides with the expression derived from Eq. (22) only at low temperatures. If $\mu_{K_1} = \mu_{K_2}$, we see again that $\alpha_{xy} = 0$, since the Berry curvature $\Pi_{K_1} = -\Pi_{K_2}$. However, the anomalous Nernst coefficient for each valley remains non-zero. The anomalous Nernst effect, for a uniform chemical potential, can therefore be used to create equal and opposite valley-index polarization on the two transverse edges. This situation is similar to the analogous spin Hall effect²⁹ or possible valley Hall effect in graphene¹⁵. For unequal chemical potential in the valleys, which can be either artificially created¹⁹ or induced by a perpendicular magnetic field in a generic Nernst set up, there will be a non-zero anomalous contribution to the Nernst effect in graphene. The unequal valley chemical potential in the presence of an external magnetic field is due to the Zeeman-type coupling of the magnetic field with the substantial magnetic moment associated with the valleys, which can be 30 times bigger than the usual spin magnetic moment¹⁵.

Since Eq. (24) is more general than the Mott relation, and may be used to go beyond the linear temperature dependence of α_{xy} (22), we numerically evaluate Eq. (24) to calculate the Nernst coefficient. We plot the anomalous Nernst coefficient as a function of μ and T for a single valley in single layer graphene in Fig. (2). In Fig. 2a, there is a nonzero Nernst

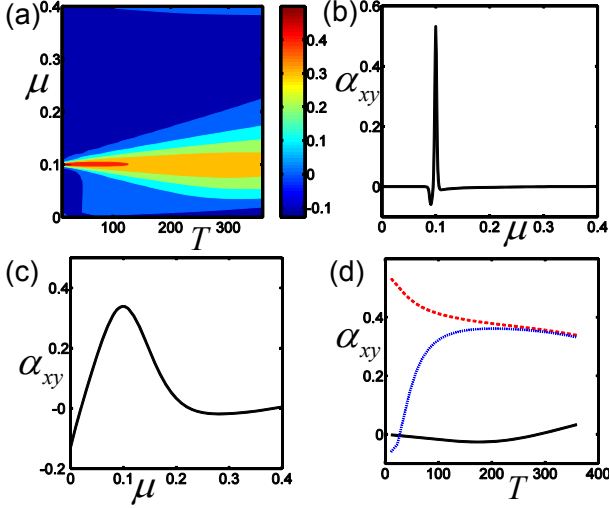


FIG. 3: (Color online) Anomalous Nernst signal for a single valley for bilayer graphene. The units for μ , T , and α_{xy} are eV, K, and $k_B e/\hbar$, respectively. The parameters $t = 2.82eV$, $V = 0.2eV$, $t_{\perp} = 0.4eV$. (a) Contour plot for α_{xy} . (b) Plot of α_{xy} with respect to μ for $T = 11.6$ K. Note the dramatic variation of α_{xy} around $\mu = V/2$. (c) Plot of α_{xy} with respect to μ for $T = 360$ K. (d) Plot of α_{xy} with respect to T for $\mu = 0.2$ eV (Solid line), 0.1 eV (Dashed line), 0.091 eV (Dotted line).

coefficient even when the chemical potential is inside the band gap, while the Mott relation yields a zero Nernst signal in this case. In Fig. 2b, Nernst conductivity α_{xy} increases sharply to a maximum, while the Mott relation yields a step jump at $\mu = \frac{\Delta}{2}$. In Fig. 2c, the step jump is further smoothed out at medium temperatures (note that T here is still much smaller than Δ). The deviation of α_{xy} from the linear temperature dependence given by the Mott relation is clearly visible in Fig. 2d.

B. Anomalous Nernst effect in bilayer graphene

The Hamiltonian for a single valley in biased bilayer graphene can be written as²⁶

$$\hat{H} = \begin{pmatrix} V/2 & tke^{i\phi_{\mathbf{k}}} & t_{\perp} & 0 \\ tke^{-i\phi_{\mathbf{k}}} & V/2 & 0 & 0 \\ t_{\perp} & 0 & -V/2 & tke^{-i\phi_{\mathbf{k}}} \\ 0 & 0 & tke^{i\phi_{\mathbf{k}}} & -V/2 \end{pmatrix} \quad (25)$$

where V is the interlayer bias voltage, t_{\perp} and t describe interlayer and intralayer nearest neighbor hoppings and $\phi_{\mathbf{k}}$ is the angle of \mathbf{k} on the 2D momentum space. The eigenenergies and eigenstates can be obtained analytically, which yield the Berry curvature for the n -th band

$$\Pi_n = \frac{1}{k} \frac{\partial}{\partial k} [A_n^2 (\gamma_{1n}^2 - \gamma_{3n}^2)]. \quad (26)$$

Here $A_n = (1 + \gamma_{1n}^2 + \gamma_{2n}^2 + \gamma_{3n}^2)^{-1/2}$, $\gamma_{1n} = tk/(E_n - V/2)$, $\gamma_{2n} = -[t^2 k^2/(E_n - V/2) - (E_n - V/2)]/t_{\perp}$, $\gamma_{3n} = \gamma_2 tk/(E_n + V/2)$, and, finally,

$$E_n = \pm \frac{1}{2} \sqrt{\frac{2t_{\perp}^2 + V^2 + 4t^2 k^2}{\pm 2\sqrt{4(V^2 + t_{\perp}^2)t^2 k^2 + t_{\perp}^4}}} \quad (27)$$

are the eigenenergies.

In Fig. 3, we plot α_{xy} as a function of μ and T , similar as in Fig. 2. Note that, in this case, α_{xy} can change sign in some regimes of the parameter space. Such sign changes are due to the complicity of the four bands of bilayer graphene. At low temperatures, $\alpha_{xy} = 0$ for $\mu < V/2$ and changes dramatically around $\mu = V/2$. The dramatic change of α_{xy} disappears at medium temperatures, but the sign change still remains (see Fig. 3c). At different chemical potentials, the temperature dependence of α_{xy} shows quite different behavior (see Fig. 3d). For uniform chemical potential at the valleys, the total anomalous Nernst signal is zero, even though, like in the case of single layer graphene, they can be substantial locally in the momentum space.

C. Conclusion

In summary, we discuss the effects of the topological Berry phases on the thermoelectric response coefficients of the Dirac-like quasiparticles in gapped single and bilayer graphene. The gap in the single layer graphene can be due to SI symmetry breaking, as claimed, for instance, in epitaxial graphene in Ref.⁹. It may also be due to confined geometries, such as in graphene nanoribbons^{10,11}. For bilayer graphene, the gap may be due to applied voltage bias¹². We show that in such samples the anomalous contribution to the Nernst effect is non-zero for a non-zero valley polarization. We also show that the nonlinear quasiparticle dispersion spectrum does not significantly change the results. A non-zero valley polarization may be artificially created¹⁹, or it can be induced by a perpendicular magnetic field due to the substantial valley magnetic moment¹⁵ in a generic Nernst set up. The regular Nernst effect in gapped graphene may, therefore, have a substantial anomalous contribution because of the valley polarization. Even in the absence of any valley polarization, the spontaneous Nernst effect from an individual valley is locally non-zero, opening up the possibility to create a measurable valley polarization on the transverse edges of a sample which can be technologically very important.

Acknowledgement: Zhang is supported by WSU startup funds. Tewari is supported by DOE/EPSCoR Grant # DE-FG02-04ER-46139 and Clemson University startup funds.

-
- ¹ A. K. Geim, and K. S. Novoselov, *Nature Mater.* **6**, 183 (2007).
 - ² A. H. Castro Neto, F. Guinea, N. M. R. Peres, K. S. Novoselov, A. K. Geim, *Rev. Mod. Phys.* **81**, 109 (2009).
 - ³ K. S. Novoselov, A. K. Geim, S. V. Morozov, D. Jiang, Y. Zhang, S. V. Dubonos, I. V. Grigorieva, and A. A. Firsov, *Science* **306**, 666 (2004).
 - ⁴ K. S. Novoselov, A. K. Geim, S. V. Morozov, D. Jiang, M. I. Katsnelson, I. V. Grigorieva, S. V. Dubonos, and A. A. Firsov, *Nature* **438**, 197 (2005).
 - ⁵ Y. Zhang Y.-W. Tan, H. L. Stormer and P. Kim, *Nature* **438**, 201 (2005).
 - ⁶ S. V. Morozov, K. S. Novoselov, M. I. Katsnelson, F. Schedin, L. A. Ponomarenko, D. Jiang, and A. K. Geim, *Phys. Rev. Lett.* **97**, 016801 (2006).
 - ⁷ A. F. Morpurgo and F. Guinea, *Phys. Rev. Lett.* **97**, 196804 (2006).
 - ⁸ R. V. Gorbachev, F. V. Tikhonenko, A. S. Mayorov, D. W. Horsell, and A. K. Savchenko, *Phys. Rev. Lett.* **98**, 176805 (2007).
 - ⁹ S. Y. Zhou G.-H. Gweon, A. V. Fedorov, P. N. First, W. A. de Heer, D.-H. Lee, F. Guinea, A. H. Castro Neto, and A. Lanzara, *Nature Mater.* **6**, 770 (2007); E. Rotenberg *et al.*, *ibid* **7**, 258 (2008); S. Y. Zhou *et al.*, *ibid* **7**, 259 (2008);
 - ¹⁰ M. Y. Han, B. Özyilmaz, Y. Zhang, and P. Kim, *Phys. Rev. Lett.* **98**, 206805 (2007).
 - ¹¹ S. Adam, S. Cho, M. S. Fuhrer, and S. Das Sarma, *Phys. Rev. Lett.* **101**, 046404 (2008).
 - ¹² T. Ohta, A. Bostwick, T. Seyller, K. Horn, and E. Rotenberg, *Science* **313**, 951 (2006).
 - ¹³ M. V. Berry, *Proc. R. Soc. London, Ser. A* **392**, 45 (1984).
 - ¹⁴ N. A. Sinitsyn, J. E. Hill, H. Min, J. Sinova, and A. H. MacDonald, *Phys. Rev. Lett.* **97**, 106804 (2006).
 - ¹⁵ D. Xiao, W. Yao, and Q. Niu, *Phys. Rev. Lett.* **99**, 236809 (2007).
 - ¹⁶ P. Wei, W. Bao, Y. Pu, C. N. Lau, and J. Shi, arXiv:0812.1411 (2008).
 - ¹⁷ Y. M. Zuev, W. Chang, and P. Kim, arXiv:0812.1393 (2008).
 - ¹⁸ J. G. Checkelsky, and N. P. Ong, arXiv:0812.2886 (2008).
 - ¹⁹ A. Rycerz, J. Tworzydło and C. W. J. Beenakker, *Nature Phys.* **3**, 172 (2007).
 - ²⁰ Y. Wang, Z. A. Xu, T. Kakeshita, S. Uchida, S. Ono, Y. Ando, and N. P. Ong, *Phys. Rev. B* **64**, 224519 (2001).
 - ²¹ M. P. Marder, *Condensed Matter Physics*, Wiley, New York, (2000).
 - ²² V. M. Yakovenko, *Phys. Rev. Lett.* **98**, 087003 (2007).
 - ²³ S. Tewari, C. Zhang, V. M. Yakovenko, and S. Das Sarma, *Phys. Rev. Lett.* **100**, 217004 (2008).
 - ²⁴ D. Xiao, Y. Yao, Z. Fang, and Q. Niu, *Phys. Rev. Lett.* **97**, 026603 (2006).
 - ²⁵ N. R. Cooper, B. I. Halperin, and I. M. Ruzin, *Phys. Rev. B* **55**, 2344 (1997).
 - ²⁶ J. Nilsson, A. H. Castro Neto, F. Guinea, and N. M. R. Peres, *Phys. Rev. B* **78**, 045405 (2008).
 - ²⁷ G. Sundaram and Q. Niu, *Phys. Rev. B* **59**, 14915 (1999).
 - ²⁸ C. Zhang, S. Tewari, V. M. Yakovenko, and S. Das Sarma, *Phys. Rev. B* **78**, 174508 (2008).
 - ²⁹ S. Murakami, N. Nagaosa, and S.-C. Zhang, *Science* **301**, 1348 (2003).